Computational Screening of Porous Carbons, Zeolites, and Metal Organic Frameworks for Desulfurization and Decarburization of Biogas, Natural Gas, and Flue Gas

Xuan Peng
Dept. of Automation, College of Information Science and Technology, Beijing University of Chemical Technology, Beijing 100029, China

State Key Laboratory of Clean Energy Utilization, Zhejiang University, Hangzhou 310027, China

Dapeng Cao
Dept. of Chemical Engineering, Div. of Molecular and Materials Simulation, State Key Laboratory of Organic-Inorganic Composites, Beijing University of Chemical Technology, Beijing 100029, P.R. China

DOI 10.1002/aic.14046
Published online February 27, 2013 in Wiley Online Library (wileyonlinelibrary.com)

Eighteen kinds of porous materials from carbons, zeolites, and metal organic frameworks (MOFs) have been extensively investigated for desulfurization and decarburization of the biogas, natural gas, and flue gas by using a molecular modeling approach. By considering not only the selectivity but also capacity, Na-5A, zeolite-like MOF (zMOF), and Na-13X, MIL-47 are screened as the most promising candidates for removal of sulfide in the CH_4—CO_2—H_2S and N_2—CO_2—SO_2 systems, respectively. However, for simultaneous removal of sulfide and CO_2, the best candidates are zMOF for the natural gas and biogas (i.e., CH_4—CO_2—H_2S system) and MOF-74-Zn for the flue gas (i.e., N_2—CO_2—SO_2 system). Moreover, the regeneration ability of the recommended adsorbents is further assessed by studying the effect of temperature on adsorption. It is found that compared to the zMOF and MIL-47 MOFs, the Na-5A and Na-13X zeolites are not easily regenerated due to the difficulty in desorption of sulfide at high temperature, which results from the stronger adsorbent–adsorbate interactions in zeolites. The effect of sulfide concentration on the adsorption properties of the recommended adsorbents is also explored. We observe that the zMOF and MIL-47 are also superior to the Na-5A and Na-13X for desulfurization of gas mixtures containing high sulfide concentration. This is because MOFs with larger pore volume lead to a greater sulfide uptake. The effects of porosity, framework density, pore volume, and accessible surface area on the separation performance are analyzed. The optimum porosity is about 0.5–0.6, to meet the requirements of both high selectivity and uptake. It is expected this work provides a useful guidance for the practical applications of desulfurization and decarburization. © 2013 American Institute of Chemical Engineers *AIChE J*, 59: 2928–2942, 2013
Keywords: adsorption/gas, computer simulations (MC and MD), decarburization, desulfurization

Introduction

In recent years, the detrimental effect of fossil fuels on human society has motivated a serious concern worldwide for the harmonious balance between energy utilization and environment protection. Generally, this issue is closely related to energy storage, carbon capture and sequestration,[1] pollutant emission control, and novel materials for these applications. As one typical energy source, raw natural gas from wellhead contains CH_4, CO_2, N_2, heavier hydrocarbons,[2,3] and hydrogen sulfide (H_2S) with a varied concentration from ppm level up to 5%.[4] Biogas is another type of energy sources that composed of 55–70% CH_4, 30–45% CO_2, trace H_2S (10–3000 ppm), and other minor components.[5] Among them, CH_4 is recognized to be an excellent alternative renewable clean energy. However, the existence of CO_2 will not only directly lead to global warming as greenhouse gas, but also reduce the energy content and particularly corrupt the transportation system in the presence of water. Consequently, CO_2 capture is another urgent challenge. For H_2S, it is reported that exposure to this toxic gas with only 300 ppm for 30 min can cause the unconscious problem to human health.[6] As is well known, the H_2 that fuel cells require is commonly produced by catalytic reforming of natural gas to synthesis gas. If the H_2S impurity in synthesis gas is not effectively reduced to a low concentration limit below 1 ppm, it will irreversibly poison the metal catalysts in both the catalytic reformers and the fuel cells electrodes.[4,7] Besides H_2S contaminant, sulfur dioxide (SO_2) constitutes another major contribution to air pollutant, which is mainly released from the combustion of coal and residual oil in power plants. The postcombustion gas, named flue gas

Additional Supporting Information may be found in the online version of this article.

Correspondence concerning this article should be addressed to X. Peng or D. Cao at pengxuan@mail.buct.edu.cn or caodp@mail.buct.edu.cn.

or stack gas, typically contains several components including N_2, 10–12% CO_2, 10–15% water vapor, 6% O_2, SO_2 (0–2000 ppm), and NO_x (100–200 ppm).[1,8–11] The emissions of sulfur gas like H_2S and SO_2 are responsible for the formation of acid rain and many other undesirable environmental and health hazards. Therefore, controlling their emission has become increasingly crucial importance on global atmospheric chemistry and quality of life.

A variety of processes have been developed to remove the sulfur before its emission into the atmosphere. For instance, the amine solution extraction[4,7] and the wet scrubbing method[11] using lime/limestone are the popular technologies for removing H_2S and SO_2, respectively. Adsorption can also be used, due to the unique advantages of less energy consumption for adsorbent regeneration, relatively simple adsorber design compared to chemical reactor, and minimum waste disposal problems.[8] If a suitable adsorbent is available, the adsorption approach would be competitive with other techniques mentioned above. A promising adsorbent should possess the characteristics of high sulfur selectivity and large capacity, mild operating temperature and pressure, good regenerability, high thermal stability, and tolerance to other impurities in the feed.[1,4] To date, a large number of novel porous materials have been synthesized and used for gas storage and separation, examples including porous carbons[3,12–17] and zeolites.[6,18–27]

Recently, considerable research efforts were made to metal organic frameworks (MOFs),[28,29] which have been regarded as the most promising microporous or/and mesoporous materials. This is because MOFs are constructed by the assembly of organic linking units with metal ions or metal clusters, and their chemical functionality and pore structures can be adjusted controllably. By tuning the length of the organic linker and varying the metal cluster, the pore volume and pore size of MOFs can be tailored over a wide atomic-scale range for special applications. These distinct advantages have substantially promoted the experimental and computational studies on the preparation and applications of MOFs.[30–37] As typical representatives, Babarao and Jiang[38] reported a molecular simulation study on CO_2 storage in ZSM-5 zeolite, single wall nanotube (SWNT), and a series of isoreticular MOFs. Similarly, Yazaydın et al.[39] screened 14 MOFs for CO_2 capture using a combined experimental and modeling approach. Hamon et al.[40,41] investigated the adsorption of H_2S and the CH_4/H_2S separation in the MIL type of MOFs. Liu and Smit[42] performed a comparative molecular simulation study of CO_2/N_2 and CH_4/N_2 separation in zeolites and MOFs. Herm et al. examined the separation of CO_2/H_2 in selected several MOFs[43] via adsorption experiment and ideal adsorbed solution theory (IAST) prediction.[44]

To the best of our knowledge, most investigations are only limited to storage of pure gases and separation of binary mixtures. However, in a practical application, the multicomponent adsorption often occurs and it is more worth studying. Unfortunately, almost no investigations were focused on the applications of desulfurization only and desulfurization/decarburization simultaneously.[45] Moreover, the experimental measurements and the macroscopic adsorption model-based theory (e.g., IAST) are quietly difficult to study the separation of mixtures containing the trace amount (ppm) sulfur gases, because it would yield the inacceptable measuring and predicting deviations. Accordingly, here we intend to use molecular simulation method to systematically explore the neglected topic.

To achieve this target, 18 kinds of porous materials were sorted from different families of carbons, zeolites, and MOFs. The ternary mixtures of CH_4—CO_2—H_2S and N_2—CO_2—SO_2 with a typical sulfide composition of 0.002 (2000 ppm) were adopted to mimic the real biogas, natural gas, and flue gas, respectively. This work is organized as follows. First, we describe the structures of porous materials, the potential models, and the details of molecular simulation. Second, we screen the adsorbents for the desulfurization and decarburization applications. Then, we investigate the effects of temperature and sulfur concentration on adsorption properties of recommended materials. Finally, we discuss the relation between structural properties of materials and separation selectivity.

Molecular Simulation

Sorting porous materials

The SWNT was selected here because it is one of the most important carbons[12] and also presents an excellent performance for capture of trace sulfur gases from binary mixtures.[46] Furthermore, our previous work indicates that another type carbon of C_{60} intercalated graphite (CIG) behaves very well for CO_2 purification, especially for N_2—CO_2 system at room temperature,[15] and therefore chosen here. As typical representatives of faujasite (FAU) and Linde type families, synthetic Na-13X,[23,24,47] Na-5A,[25,48,49] and Na-4A[18,20,22,26,27] zeolites are considered here for their widespread use as molecular sieves and cation exchangers in catalysis and separation processes. MOF-5,[29,50] HKUST-1,[28] MIL-47(V),[40,41,51,52] MOF-177,[53,54] and COF-102[55–58] are selected because they are the hot topic materials and could be candidates for gas storage and separation. NOTT-103[59] incorporates a vacant coordination site at Cu(II) centers and has large pore volumes that contribute to high gas adsorption. ZIF-3[60,61] exhibits significantly higher adsorption and permeation selectivities for separation of gas mixtures compared to widely studied MOF membranes.[62] For ZIF-96, the nitrile and amine functional groups on the imidazolate linker lead to high CO_2 uptake,[63] and we conjecture that it may be a good candidate for the separation of sulfide gas. The MOF-74-M series (M=Zn, Ni, Co)[64–67] with the same crystal structures and different unsaturated coordinative metal centers present an ideal system to explore the roles of open metals in separation of the polar and nonpolar gas mixtures. Soc-MOF[68] and *rho*-zMOF[69] are selected because they exhibit unprecedentedly high selective adsorption for the CO_2/CH_4 and CO_2/N_2 mixtures among various MOFs and nanoporous materials.[70,71]

Material structures

As mentioned previously, SWNT bundle was constructed in a diamond-like structure,[46] whereas CIG was built by intercalating the hexagonally aligned fullerene into three parallel graphite planes.[15] Zeolite 13X is composed of sodalite units interconnected through six-membered oxygen bridges (hexagonal prisms) to form a cubic lattice of supercages $\sim$12.5 Å in diameter.[24] These supercages are tetrahedrally linked through 12-membered-ring windows about 7.4 Å in width.[24] Different number of Na^+ cations can be exchanged into zeolite 13X to counterbalance the negative charges due to the Al/Si substitution in the framework. In this work, 88 Na^+ cations per unit cell were used to represent zeolite 13X,

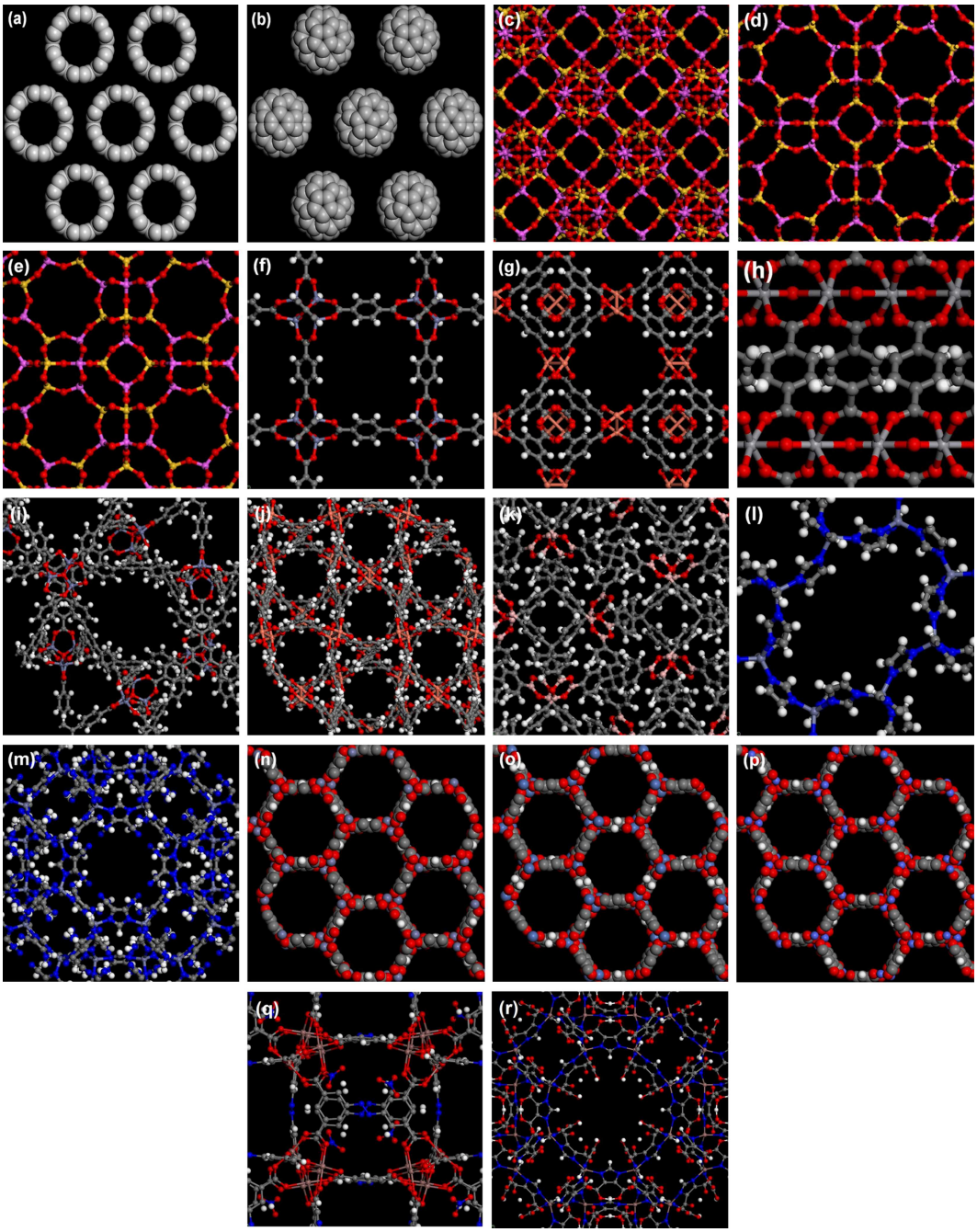

Figure 1. Material structures of (a) SWNT, (b) CIG, (c) Na-13X, (d) Na-5A, (e) Na-4A, (f) MOF-5, (g) HKUST-1, (h) MIL-47(V), (i) MOF-177, (j) NOTT-103, (k) COF-102, (l) ZIF-3, (m) ZIF-96, (n) MOF-74-Zn, (o) MOF-74-Ni, (p) MOF-74-Co, (q) soc-MOF, and (r) zMOF.

All the Na^+ and Ca^{2+} ions are hidden for clarity. [Color figure can be viewed in the online issue, which is available at wileyonlinelibrary.com.]

which yields a chemical composition of $Na_{88}Al_{88}Si_{104}O_{384}$. The structure of Na-13X was obtained from the reported fractional coordinates of NaX(0)[72] by randomly replacing Si by Al atoms to satisfy the Löwenstein rule, that is, all Al atoms link to 4 Si atoms via 4 O atoms and the framework Si and Al strictly alternates.[49] Zeolites 5A and 4A are also often synthesized in the sodium form, belonging to a family of LTA-type zeolites. Their crystal unit cell consists of eight spherical α-cages of $\sim$11.2 Å interconnected via windows of $\sim$4.1 Å in diameter.[49] The Si/Al ratio of both zeolites is approximately equal to 1, and the composition of zeolite 4A is $Na_{96}Al_{96}Si_{96}O_{384}$, whereas the composition of zeolite 5A is $Na_{32}Ca_{32}Al_{96}Si_{96}O_{384}$, which is obtained by using 32 Ca^{2+} and 32 Na^+ cations per unit cell, corresponding to a postsynthesis exchange by replacing the Na^+ with Ca^{2+} cations experimentally. The crystal positions from Subramanian and Seff[26] and Pluth and Smith[48] were used for the constructions of zeolites Na-4A and Na-5A, respectively.

For MOF-5, each oxide-centered Zn_4O tetrahedron is edge-connected by six 1,4-benzenedicarboxylate linkers to form a cubic topology with cavity diameter of 14 Å.[29,50] As to HKUST-1, copper dimers as four connectors and benzene-1,3,5-tricarboxylate as three connectors constitute $Cu_2(COO)_4$ paddle wheels to form a three-dimensional (3-D) network with main channels of a square cross-section of 9 Å diameter and tetrahedral side pockets of 5 Å, which are

Table 1. Summary of Structural Properties for Porous Materials[a]

No.	Materials	Unit cell (Å)	Cell angle (°)	Number of unit cells	ρ_f (g cm^{-3})	V_{free} (cm^3 g^{-1})	ϕ	S_a (m^2 g^{-1})
1	SWNT (6,6)	a = 12.14, b = 21.027, c = 27.05	$\alpha=\beta=\gamma$ = 90	4 × 3 × 2	1.53	0.25	0.38	197.7[b]
2	CIG	a = 25.0, b = 21.65, c = 25.4	$\alpha=\beta=\gamma$ = 90	2 × 3 × 2	1.57	0.29	0.46	343.2[b]
3	Na-13X	$a=b=c$ = 25.092	$\alpha=\beta=\gamma$ = 90	2 × 2 × 2	1.42	0.39	0.55	924.1[b]
4	Na-5A	$a=b=c$ = 24.555	$\alpha=\beta=\gamma$ = 90	2 × 2 × 2	1.51	0.35	0.53	721.0[b]
5	Na-4A	$a=b=c$ = 24.584	$\alpha=\beta=\gamma$ = 90	2 × 2 × 2	1.52	0.33	0.51	710.6[b]
6	MOF-5	$a=b=c$ = 25.832	$\alpha=\beta=\gamma$ = 90	2 × 2 × 2	0.59	1.35	0.80	3365.1[c]
7	HKUST-1	$a=b=c$ = 26.343	$\alpha=\beta=\gamma$ = 90	2 × 2 × 2	0.88	0.80	0.71	2134.0[c]
8	MIL-47(V)	a = 6.818, b = 16.143, c = 13.939	$\alpha=\beta=\gamma$ = 90	6 × 3 × 4	1.0	0.61	0.61	1511.7[c]
9	MOF-177	$a=b$ = 37.072, c = 30.033	$\alpha=\beta$ = 90, γ = 120	1 × 1 × 1	0.43	1.93	0.82	4833.0[c]
10	NOTT-103	$a=b$ = 18.513, c = 45.354	$\alpha=\beta$ = 90, γ = 120	2 × 2 × 1	0.64	1.15	0.74	3646.4[b]
11	COF-102	$a=b=c$ = 27.177	$\alpha=\beta=\gamma$ = 90	2 × 2 × 2	0.42	1.83	0.77	5129.5[b]
12	ZIF-3	$a=b$ = 18.97, c = 16.74	$\alpha=\beta=\gamma$ = 90	2 × 2 × 2	0.88	0.75	0.66	1902.3[b]
13	ZIF-96	$a=b=c$ = 28.3564	$\alpha=\beta=\gamma$ = 90	1 × 1 × 1	0.98	0.60	0.59	1197.1[b]
14	MOF-74-Zn	$a=b$ = 25.932, c = 6.837	$\alpha=\beta$ = 90, γ = 120	2 × 2 × 4	1.22	0.54	0.65	1324.4[c]
15	MOF-74-Ni	$a=b$ = 25.786, c = 6.77	$\alpha=\beta$ = 90, γ = 120	2 × 2 × 4	1.19	0.54	0.64	1456.3[c]
16	MOF-74-Co	$a=b$ = 26.11, c = 6.719	$\alpha=\beta$ = 90, γ = 120	2 × 2 × 4	1.18	0.55	0.65	1508.2[c]
17	soc-MOF	$a=b=c$ = 22.457	$\alpha=\beta=\gamma$ = 90	2 × 2 × 2	1.12	0.57	0.64	1441.2[b]
18	zMOF	$a=b=c$ = 31.062	$\alpha=\beta=\gamma$ = 90	1 × 1 × 1	1.19	0.51	0.61	1069.1[b]

[a]ρ_f is the framework density, V_{free} is the free pore volume, and ϕ is the porosity expressed by the ratio of the free volume of adsorbent accessible to gas molecules to the adsorbent volume. In the present work, the free volume is calculated by a Monte Carlo integration with the reentrant surface definition,[15,74] where the argon molecule with a size of 3.4 Å was used as a probe. S_a is the accessible surface area calculated by the method of Düren et al.,[75] where the nitrogen probe with a diameter of 3.681 Å was used.
[b]This work.
[c]From the work of Yazaydin et al.[39]

linked to the main channels by triangular windows of 3.5 Å diameter.[28] Isostructural MIL-47(V) is built up from corner-sharing $V^{4+}O_6$ octahedra interconnected by terephthalate groups, forming a 3-D framework with a one-dimensional (1-D) diamond-shaped channels of diameter ~8.5 Å.[51] MOF-177 material consists of tetrahedral $[Zn_4O]^{6+}$ clusters linked by the tritopic linker 1,3,5-benzenetribenzoate, with a very high surface area about 4500 m^2 g^{-1}.[53] NOTT-103 is an isostructural polymers of composition $C_{35}H_{43}Cu_2N_3O_{16}$, which contains binuclear Cu(II) paddlewheel nodes each bridged by four carboxylate centers to yield a NbO-type network.[59] COF-102 has a cubic structure constructed completely from strong covalent bonds by joining of the triangular and tetrahedral nodes, with a crystal density 0.41 g cm^{-3} and a largest cavity of 5.66 Å.[56,73] ZIF-3 framework, consisted of zinc and imidazolate linkers, has a zeolite DFT topology,[60] whereas ZIF-96, built from the functionalized imidazoles $C_4H_4N_4$ cyamIm linker, is based on the zeolite RHO topology.[63] MOF-74-M (M═Zn, Ni, Co) is composed of M^{+2} cation bridged by the carboxylate and oxy- groups of fully deprotonated 2,5-dihydroxybenzene-1,4-dicarboxylic acid, having linked chains that are arranged in a parallel and hexagonal 1-D pore (diameter ~12 Å).[64–67] The metal centers are bonded to five oxygen atoms in a square-pyramid coordination. socMOF is synthesized by an indium trimer building block, resulted in a narrow pore diameter of about 12 Å, a composition of $[In_3O(C_{16}N_2O_8H_6)_{1.5}]$-$(NO_3)$, and a soc topology characterized by its square-octahedral connectivity net.[68] The ionically bound nitrate anions proximal to the indium trimer give the framework a highly ionic character. *rho*-zMOF, a representative of zeolite-like MOFs (zMOFs) with a topology of *rho*-zeolite used in this work, is synthesized by metal-ligand-directed assembly of In atoms and 4,5-imidazoledicarboxylic acid (H3ImDC).[69] It is obtained by substituting oxygen atoms in zeolites by organic linkers, so the structure is similar to inorganic zeolites but with an extra-large cavities size of 18.2 Å. zMOFs contain the charged frameworks and charge-balancing extra framework ions that can increase the interactions with guest molecules and consequently enhance the storage and separation capability of this material. A canonical ensemble MC simulation at 303 K was performed to characterize the locations of Na^+ ions in zMOF. Initially, 48 Na^+ ions were inserted randomly into the system followed by 10^7 trial displacement moves. The acceptance criteria for the trial moves were based on the Metropolis algorithm. All the structures of the selected MOFs were constructed from their corresponding experimental XRD data, and the CIF format files can be downloaded from the Cambridge Crystallographic Data Centre. The atomic structures of all the adsorbents are shown in Figure 1, and their lattice constants, crystal densities, pore volumes, and porosities are summarized in Table 1.

Force fields

The fluid-fluid interactions of the species are composed of the Lennard–Jones (LJ) and electrostatic interactions. In the present work, we used the same potential models for fluids as our previous work,[46] that is, the spherical united-atom LJ model to represent N_2 and CH_4, and three-site rigid model to represent CO_2, H_2S, and SO_2. Generally speaking, the united-atom LJ model (namely, one-site model) can save much computational time compared to the all-atom model, and thus is preferentially chosen if the computational accuracy can be maintained. Our recent study[76] on adsorption properties of the UMCM-1 material indicates that the simulated CH_4 isotherms with the one-site model can reproduce well the corresponding experimental data, and in particular, the one-site model is more accurate than the three-site model for N_2. Here, we used the one-site potential parameters from Babarao et al.[77] for CH_4 and Peng et al.[13] and Kaneko and coworkers[78] for N_2. In the three-site rigid models for CO_2, H_2S, and SO_2, a three-site LJ potential plus a set of partial

point charges are distributed at three electrostatic sites. The linear CO_2 molecule was described by the elementary physical model,[79,80] where the C—O bond length is 1.149 Å, the partial point charge on the C atom is +0.6512e, and electric neutrality is maintained the partial charge of −0.3256e on O atom. The H_2S molecule was represented by the three-site model from Nath's work,[81] in which the H—S bond length and H—S—H bond angle are 1.365 Å and 91.5°, with the point charges of +0.124e and −0.248e on H and S sites. Similarly, in Ribeiro's potential model[82] for SO_2 molecule, the S—O bond length and the O—S—O bond angle are 1.4321 Å and 119.5°, and the partial charges on S and O atoms are +0.470e and −0.235e.

For porous carbons, the size and energy parameters of 3.4 Å and 28.0 K were used for the carbon atom in SWNT and CIG adsorbents. In all the three zeolites, only electrostatic potential was taken into account for the interactions between the adsorbates and the framework Si and Al atoms.[22,24,49] In addition, for the O atom in zeolites, the LJ parameters of 2.806 Å and 89.6 K from Goj et al.[22] were used, whereas for Na^+ ions, 2.85 Å and 8.0 K were taken from Akten et al.[18] In Na-5A zeolite, the LJ parameters and point charge were given as 3.037 Å, 50.0 K, and +2e for Ca^2+ ions according to Ohba et al.[83] The partial charges associated with other framework atoms refer to the work of Granato et al.,[24] García-Pérez et al.,[49] and Akten et al.[18] for Na-13X, Na-5A, and Na-4A, respectively. The dispersive interactions of all the atoms in MOFs are described by directly applying the universal force field (UFF) from Rappe et al.,[84] rather than using the one that has been validated in the literatures or refining the potential parameters ourselves. This is based on the following three considerations. First, in the case of without refinement, UFF also yields a good representation of the measured adsorption isotherms for the MOFs.[76,77] Second, the refinement strategy should be executed for every adsorbate–adsorbent interaction to meet the consistency principle of force field development, not limited to the systems with available experimental data only. Unfortunately, almost no experimental adsorption data of H_2S and SO_2 in MOFs is available. Third, the experimental isotherms reported by different research groups may also vary for the same gas due to the differences of the MOFs sample preparation and activation.[39] The Na^+ ions in zMOF have the LJ parameters and partial point charge of 2.658 Å, 15.09 K, and +1e, which are the same as Babarao and Jiang.[71] For MOF-5, HKUST-1, MIL-47(V), MOF-177, and MOF-74 series, the charge data from Yazaydın et al.[39] were used here, whereas for COF-102, soc-MOF, and zMOF adsorbents, they are taken from Babarao et al.[70] and Babarao and Jiang's[71,73] works. For ZIF series, we adopted the charge from Keskin[62] and Morris et al.[63] for ZIF-3 and ZIF-96, respectively. For NOTT-103 material, *ab inito* calculations were performed using the Gaussian 03 software[85] to calculate the point charges of the atoms in the framework (see Figure S0 in Supporting Information for details). All the force field parameters were summarized in Table 2 and the Lorentz–Berthelot combining rules were used to calculate the cross LJ interactions.

Table 2. Force Field Parameters for Adsorbates and Adsorbents

Adsorbate	Atom	σ (Å)	ε/k^b (K)	q (e)	Angle (°)	[a]bl (Å)
N_2		3.549	94.95			
CH_4		3.73	148.0			
CO_2	C	2.789	29.66	+0.576	180	1.18
	O	3.011	82.96	−0.288		
H_2S	H	0. 98	3.9	+0.124	91.5	1.365
	S	3.72	250.0	−0.248		
SO_2	S	3.585	154.4	+0.470	119.5	1.4321
	O	2.993	62.3	−0.235		
Carbons	C	3.4	28.0			
Zeolites	O	2.806	89.6	[a]		
	Na	2.85	8.0	[a]		
	Ca	3.037	50.0	[a]		
MOFs	C	3.431	52.791	[a]		
	H	2.571	22.122	[a]		
	O	3.118	30.166	[a]		
	N	3.261	34.722	[a]		
	B	3.638	90.498	[a]		
	V	2.801	8.051	[a]		
	Zn	2.462	62.343	[a]		
	Cu	3.114	2.516	[a]		
	Co	2.559	7.045	[a]		
	Ni	2.525	7.548	[a]		
	Na	2.658	15.09	[a]		
	In	3.976	301.429	[a]		

[a]bl is the bond length. The partial charges for atoms on porous material are given in the text.

Simulation details

Grand canonical Monte Carlo (GCMC) simulations[86,87] were performed to investigate the adsorption and separation of gases in porous materials. During the simulations, the adsorbents were treated as a rigid material with atoms frozen. The periodic boundary conditions were imposed in three dimensions to mimic the crystal periodicity. The spherical cutoffs of 12.0 Å for carbon/zeolites and 12.8 Å for MOFs were used to calculate the intermolecular LJ interactions without long-range corrections.[42] For orthogonal systems, the electrostatic interaction between adsorbate and adsorbent was handled by using the Ewald summation technique, whereas for non-orthogonal systems and the electrostatic interaction between adsorbates, Wolf spherically truncated method[88] was used and the cutoff was set as the same as that of the LJ interactions. To accelerate the simulation, the LJ and electrostatic interactions between adsorbate and adsorbent were interpolated from a pretabulated energy map with a grid spacing 0.2 Å. A total of 2×10^7 configurations were generated for each pressure point. The first 1×10^7 configurations were discarded to guarantee equilibration and the second one was divided into 20 blocks to calculate the ensemble average. For N_2 and CH_4 with sphere geometry, only three types of moves including translation, insertion, and deletion are attempted, whereas for other molecules with three-site potential models, an additional rotation move is implemented. All the GCMC simulations were conducted by using the MUSIC code.[89] The normal move acceptance probability is transformed to relate the component fugacity of bulk phase by Peng–Robinson equation of state (PR EOS).[90] Therefore, the fugacity rather than chemical potential is used as an input parameter in the simulations. The critical properties and the binary interaction parameters of PR EOS are given in Supporting Information Table S1.

All the uptakes are reported as the absolute adsorption amount. To investigate the separation ability of porous material for gas mixtures, we defined three adsorption selectivities as follows

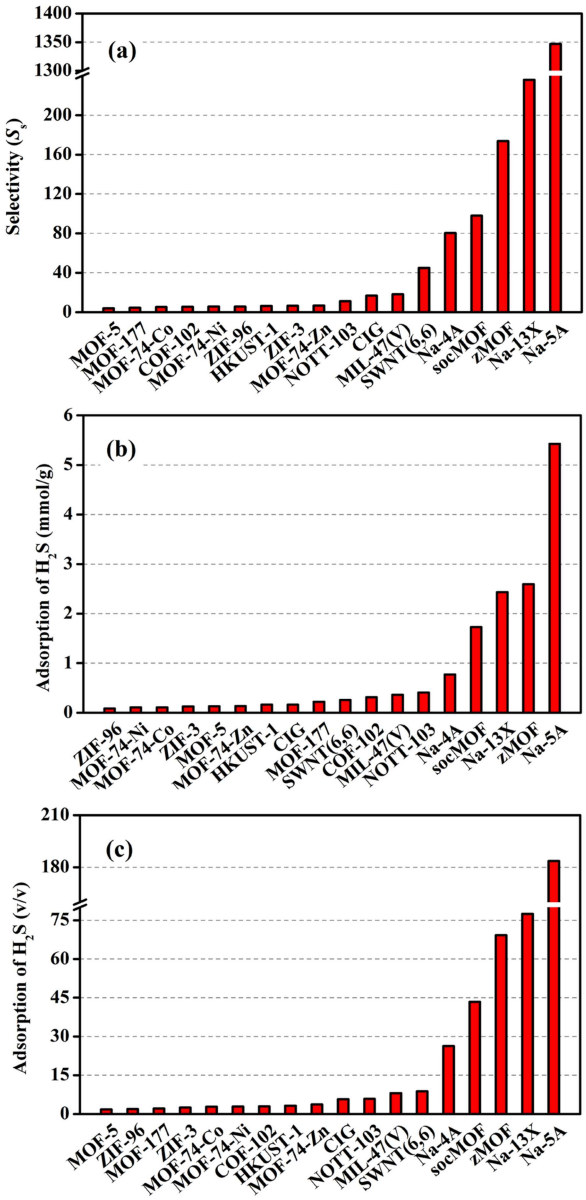

Figure 2. Removal of sulfide from the CH_4—CO_2—H_2S system ($y_{CH_4} = 0.7$ and $y_{H_2S} = 0.002$) in the recommended porous materials at 4 MPa and 303 K.

[Color figure can be viewed in the online issue, which is available at wileyonlinelibrary.com.]

$$S_{i/j} = \frac{x_i/x_j}{y_i/y_j} \tag{1}$$

$$S_s = \frac{x_s(1-y_s)}{y_s(1-x_s)} \tag{2}$$

$$S_{sc} = \frac{(x_s+x_{co_2})(1-y_s-y_{co_2})}{(y_s+y_{co_2})(1-x_s-x_{co_2})} \tag{3}$$

where $S_{i/j}$ refers to the selectivity of the first component i over the second component j, S_s denotes the desulfurization ability stand alone, S_{sc} denotes the desulfurization and decarburization ability simultaneously, the subscript S means the sulfide gas of H_2S or SO_2, and the x, y denote the molar fractions of species in the adsorbed and bulk phases, respectively.

Results and Discussions

Pairwise adsorption selectivities and the component isotherms

As mentioned before, we first consider the removal of trace sulfur of biogas, which mainly contains CH_4, CO_2, and H_2S, and postcombustion flue gas which mainly contains N_2, CO_2, and SO_2, and therefore, investigate the two corresponding ternary mixture systems and the pairwise adsorption selectivity in the two ternary mixture systems. Supporting Information Figures S1–S18 show the pairwise adsorption selectivities and the component isotherms of CH_4—CO_2—H_2S and N_2—CO_2—SO_2 systems in 18 materials of MOF-5, HKUST-1, MIL-47(V), ZIF-3, ZIF-96, COF-102, MOF-177, NOTT-103, SWNT(6,6), CIG, Na-13X, Na-5A,

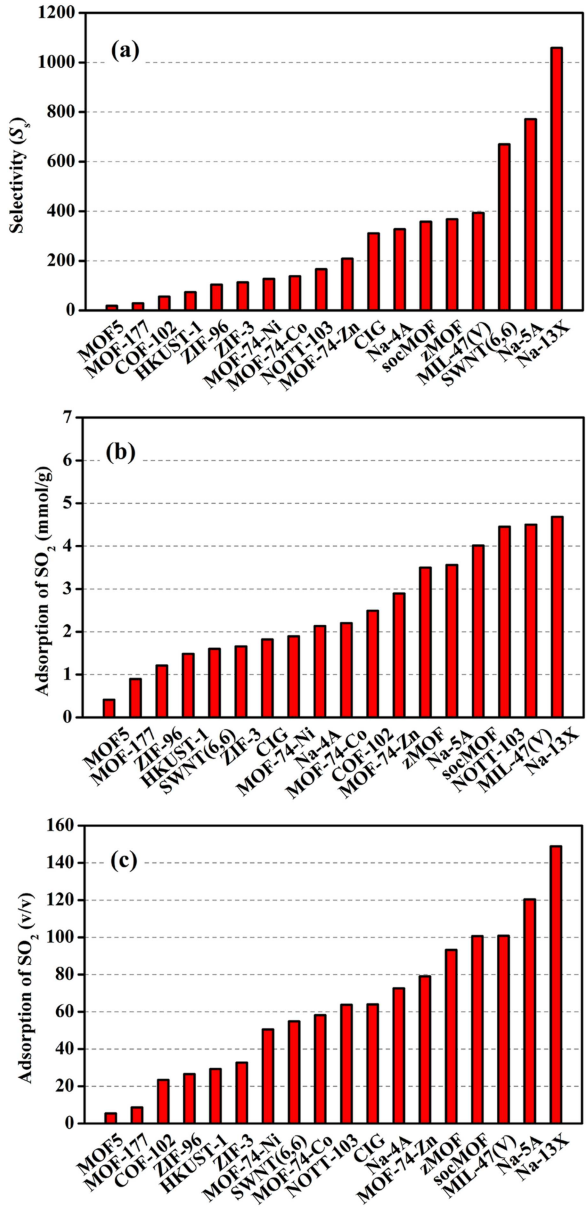

Figure 3. Removal of sulfide from the N_2—CO_2—SO_2 system ($y_{N_2} = 0.8$ and $y_{SO_2} = 0.002$) in the recommended porous materials at 4 MPa and 303 K.

[Color figure can be viewed in the online issue, which is available at wileyonlinelibrary.com.]

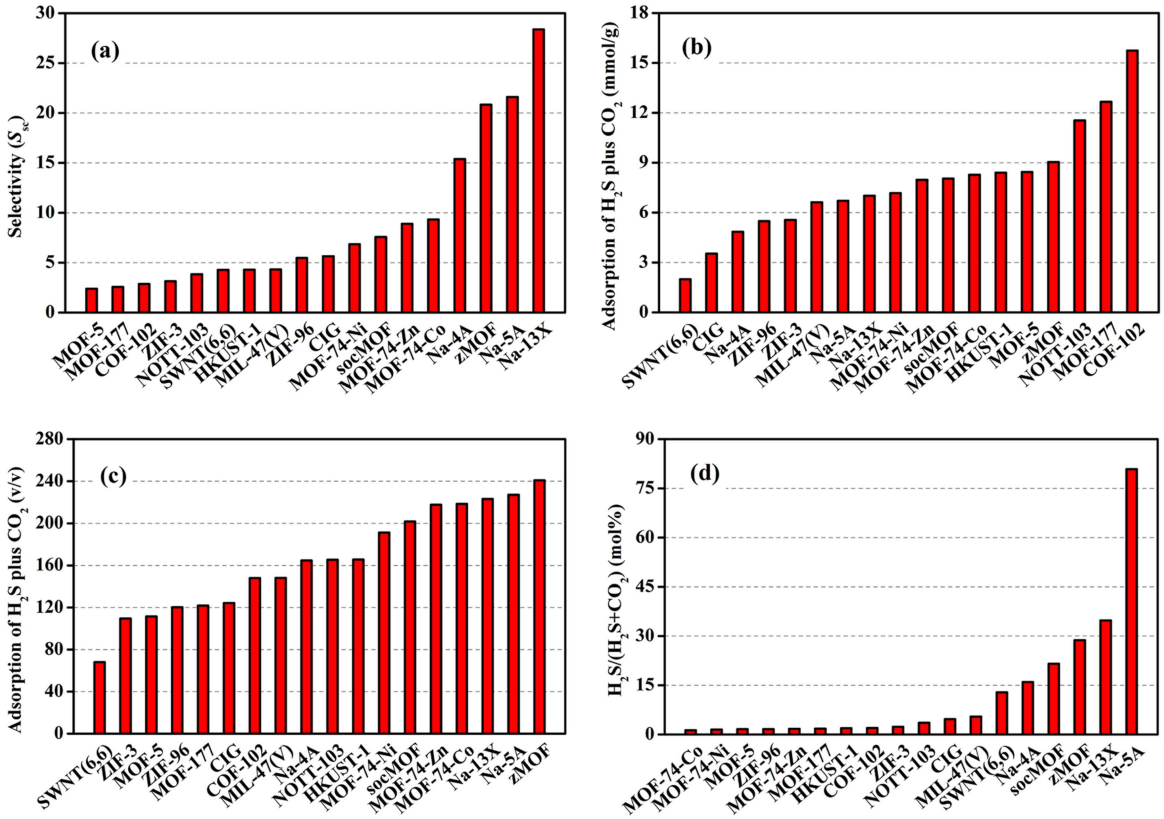

Figure 4. Simultaneous removal of sulfide and CO_2 from the CH_4—CO_2—H_2S system ($y_{CH_4} = 0.7$ and $y_{H_2S} = 0.002$) in the recommended porous materials at 4 MPa and 303 K.

[Color figure can be viewed in the online issue, which is available at wileyonlinelibrary.com.]

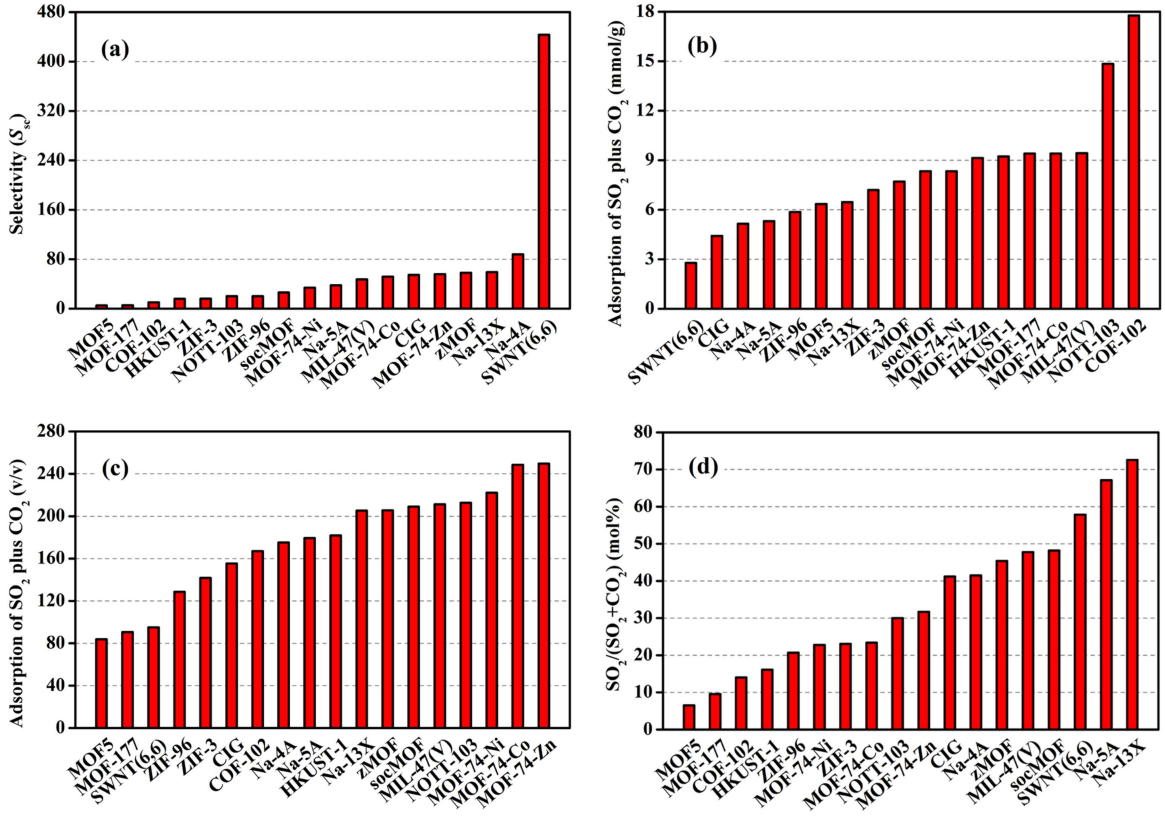

Figure 5. Simultaneous removal of sulfide and CO_2 from the N_2—CO_2—SO_2 system ($y_{N_2} = 0.8$ and $y_{SO_2} = 0.002$) in the recommended porous materials at 4 MPa and 303 K.

[Color figure can be viewed in the online issue, which is available at wileyonlinelibrary.com.]

Table 3. Recommended Porous Materials for Removal of Sulfide only and Simultaneous Removal of Sulfide and CO_2

System	Removal of sulfide	Simultaneous removal of sulfide and CO_2
Biogas and nature gas (CH_4—CO_2—H_2S)	Na-5A, zMOF	zMOF
Flue gas (N_2—CO_2—SO_2)	Na-13X, MIL-47	MOF-74-Zn

Na-4A, MOF-74-Zn, MOF-74-Co, MOF-74-Ni, socMOF, and zMOF at 303 K, respectively, where the bulk gas molar ratio of the CH_4—CO_2—H_2S system is 0.7:0.298:0.002; whereas that of the N_2—CO_2—SO_2 system is 0.8:0.198:0.002. Apparently, the selectivity of H_2S/CH_4 in the CH_4—CO_2—H_2S system and the one of SO_2/N_2 in the N_2—CO_2—SO_2 system are always the largest, because H_2S and SO_2 are the most preferentially adsorbed, whereas CH_4 and N_2 are the most unfavorably adsorbed in their corresponding ternary mixtures. Accordingly, these selectivities span several orders of magnitude from 10 to 10^6 for different pairwises. Furthermore, the shapes of the selectivity curves exhibit apparently different behavior such as monotonically ascending or descending with the increase of pressure, which is strongly dependent on the types of the materials. However, at high pressure the selectivities gradually reach a stable plateau. Among the species of ternary mixtures, CO_2 almost occupies the largest adsorption capacity for all the adsorbents, except that the uptakes of sulfide gases are the greatest in SWNT and Na-13X for N_2—CO_2—SO_2 and in Na-5A for both systems. In the latter, the sulfide uptake quickly reaches saturation at low pressure near zero, indicating that the adsorption isotherms can be classified as type I for micropore filling. These observations above give us a chance to screen the more suitable candidate for desulfurization and decarburization of biogas and postcombustion flue gas.

Screening adsorbents for removal of sulfide only

To evaluate the separation ability of various adsorbents, the adsorption data at 4 MPa are chosen to obtain the optimization for both the uptake and the selectivity, because the pressure is acceptable for industrial applications. Figures 2 and 3 show the desulfurization selectivity alone of S_s, and the sulfide uptakes in both gravimetric and volumetric units for CH_4—CO_2—H_2S and N_2—CO_2—SO_2 systems, respectively. For H_2S removal, zMOF, socMOF and all the three zeolites dominate the top five for both selectivity and uptake (see Figure 2), which is because all the five adsorbents have intrinsic ionic characteristics which can enhance the material affinity towards guest molecules. Among them, Na-5A ranks the first and especially its S_s is 4.7 times more than the second one of Na-13X, reaching up to an extraordinary high value of 1347. The big difference between both adsorbents is mainly derived from the fact that Na-5X contains two types of Na^+ and Ca^{2+} ions which can simultaneously contribute to the adsorption of H_2S. Nevertheless, only Na^+ ions are included in Na-13X and thus the greater desulfurization

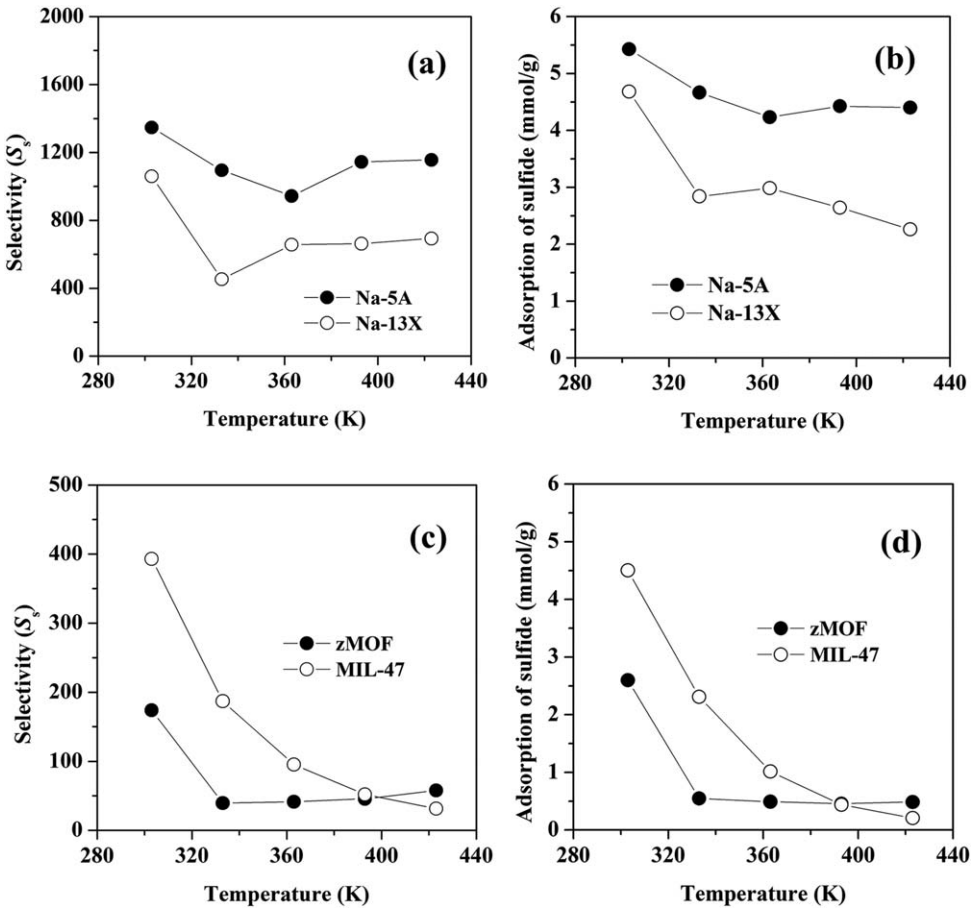

Figure 6. Effect of temperature on removal of sulfide in the recommended porous materials at 4 MPa, where the closed and open symbols denote the CH_4—CO_2—H_2S and N_2—CO_2—SO_2 systems, respectively.

selectivity is anticipated to be Na-5X, despite that both of them belong to the same family of zeolite.

Besides the ionic characteristic of adsorbents, another factor that affects the sulfide purification is the confinement effect (i.e., pore size and volume of a porous material) and functionalization of the surface. This is typically reflected in SWNT and CIG materials. Since there is no modification of polar functional groups on the smooth surface of these carbons, these carbons are not the best for the desulfurization. However, we can see from Figure 2 that their selectivities and uptakes are even better than several MOFs like HKUST-1 and ZIF-96, which possess the exposed metal centers or polar functional groups to favor the adsorption separation. This can be explained by the fact that both SWNT and CIG have very small micorpore, which is less than half of HKUST-1 and ZIF-96 in pore volume (see Table 1). That is to say, in this case, the confinement effect of the two carbon materials is stronger, and accordingly it plays an important role in determining the separation ability.

As shown in Figure 2, among the top five adsorbents, zMOF is superior to socMOF and Na-4A in both selectivity and uptake. Although its selectivity is about 26% lower than that of Na-13X, its volumetric uptake is comparable to Na-13X, and zMOF even exceeds Na-13X in the gravimetric uptake. Therefore, Na-5A from zeolites family and zMOF from MOFs family are recommended for H_2S removal. For SO_2 removal, the top five selectivity S_s is Na-13X > Na-5A > SWNT > MIL-47(V) > zMOF (see Figure 3a). Different from H_2S removal, here Na-13X exhibits the greatest selectivity rather than Na-5A. The reason is that SO_2 has a bigger molecule size than H_2S (see Table 2), and therefore Na-13X with a slightly larger pore volume (see Table 1) can accommodate more number of SO_2 molecules. The uptake data in Figure 3b and c also convince this point of view. The selectivity of SWNT is only less than that of Na-13X and Na-5A. However, its gravimetric uptake falls into the bottom and thus it is excluded from the recommended list. The selectivity of MIL-47(V) is only a half of Na-5A, but it has a considerably high selectivity of 393, which is better than zMOF for desulfurization. More importantly, MIL-47(V) has the second greatest gravimetric uptake after Na-13X and is about 21% higher than that of Na-5A. As a consequence, to remove the SO_2 impurity in N_2—CO_2—SO_2 system, we recommend Na-13X and MIL-47(V) materials from zeolites and MOFs families.

Screening adsorbents for removal of sulfide and CO_2 simultaneously

Figures 4 and 5 present the sulfide, CO_2 uptakes and the selectivities S_{sc} of desulfurization and decarburization simultaneously in CH_4—CO_2—H_2S and N_2—CO_2—SO_2 systems, respectively. We can see from Figure 4a that the descending order of the top five S_{sc} is Na-13X, Na-5A, zMOF, Na-4A, and MOF-74-Co. By contrast, the descending order of sulfide and CO_2 uptake is COF-102, MOF-177, NOTT-103, zMOF, and MOF-5 (see Figure 4b). For the latter (i.e. the second list), all the zeolites are excluded because their gravimetric uptakes are lower than a half of these MOF and COF materials. Similarly, COF-102, MOF-177, NOTT-103, and MOF-5 are eliminated from the first list for their worse selectivities S_{sc}. Although the gravimetric uptake of MOF-74-Co is slightly smaller than zMOF, the selectivity of zMOF is almost twice of the former, and therefore MOF-74-Co is also not recommended. Clearly, in the two lists, only zMOF adsorbent can satisfy the requirements of both selectivity and uptake. It should be noted that zMOF also owns the best volumetric uptake of 240 v/v (see Figure 4c), which is exactly consistent with the above conclusions. Figure 4d shows the mole percentages of H_2S in the H_2S and CO_2 total uptake. It is found that H_2S adsorption is absolutely dominant in

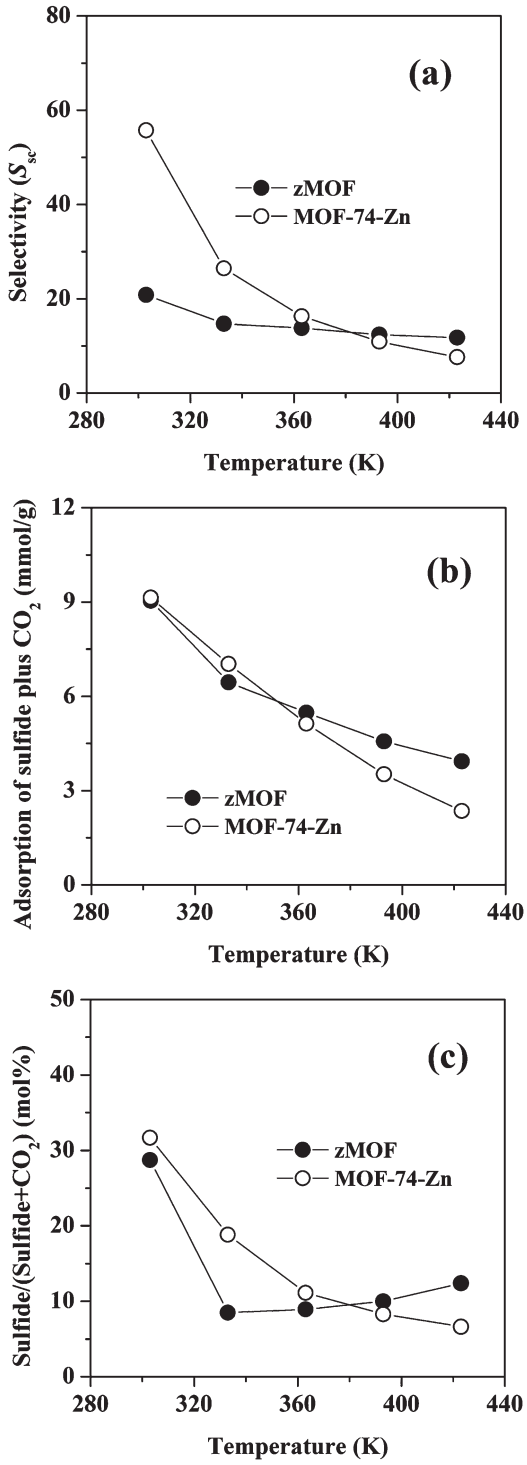

Figure 7. Effect of temperature on removal of sulfide and CO_2 in the recommended porous materials at 4 MPa, where the closed and open symbols denote the CH_4—CO_2—H_2S and N_2—CO_2—SO_2 systems, respectively.

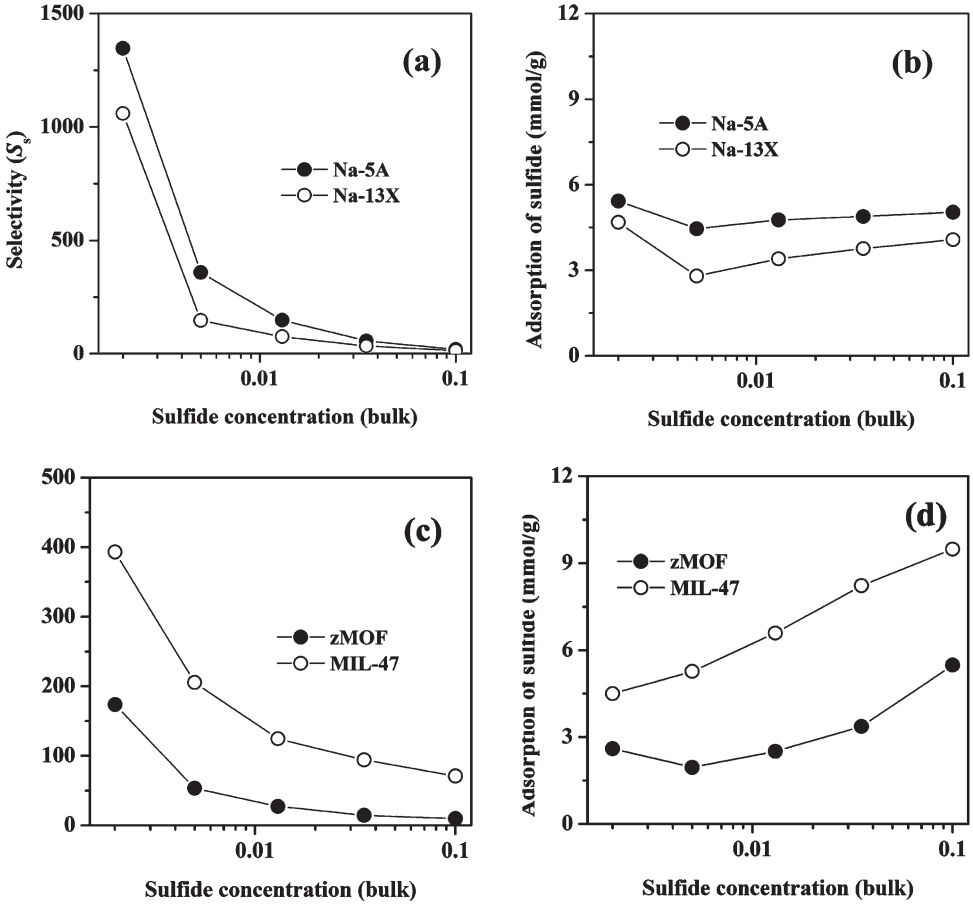

Figure 8. Effect of sulfide mole fraction in bulk phase on removal of sulfide in the recommended porous materials at 4 MPa, where the closed and open symbols denote the CH_4—CO_2—H_2S and N_2—CO_2—SO_2 systems, respectively.

Na-5A and occupies 80.9% of the total uptake. On the contrary, except H_2S, CO_2 is the major constituent in the zMOF pore, reaching 71.3% of the total uptake. Considering the trace H_2S concentration in the bulk phase, it seems that zMOF shows a good purifying ability for both H_2S and CO_2 gases. For most adsorbents of from MIL-47(V) to MOF-74-Co, the H_2S amounts are less than 5.4%, indicating that these materials give priority to decarburization other than desulfurization.

As shown in Figure 5a, for the N_2—CO_2—SO_2 system, the descending order of the top five S_{sc} is SWNT, Na-4A, Na-13X, zMOF, and MOF-74-Zn. In particular, due to the strong confinement effect, SWNT exhibits an extremely high selectivity of 443, about five times of the second one of Na-4A. In the view of gravimetric uptake, COF-102 is the best and the following is NOTT-103. Moreover, the materials from MIL-47(V) to MOF-74-Zn belong to the same level, because their uptakes approximate to each other and are around 9 mmol g^{-1}. Applying the similar screening strategy mentioned above, we only keep MOF-74-Zn, MOF-74-Co, and MIL-47(V) in the two lists. A further observation on Figure 5a and c shows that among the three adsorbents, MIL-47(V) is the worst at the selectivity and volumetric uptake, and it thus is not recommended. Meanwhile, MOF-74-Zn has a better selectivity and volumetric uptake and a slightly lower gravimetric uptake, compared to MOF-74-Co. Consequently, we propose that MOF-74-Zn is a more promising adsorbent for simultaneous removal of SO_2 and CO_2. Figure 5d shows the percentages of SO_2 in the SO_2 and CO_2 total uptake. Interestingly, we found some similar behavior as in the CH_4—CO_2—H_2S system. First, the adsorbent with the greatest sulfide percentage, in which the sulfide is absolutely preferentially adsorbed, may be not appropriate for decarburization and desulfurization. For example, here Na-13X has a 72.6% SO_2 content in the total uptake. Second, a suitable adsorbent for simultaneous removal of sulfide and CO_2 usually can reach a compromise between the competitive adsorptions of both species. In other words, it not only adsorbs a major of CO_2 molecules, but also contains a certain capacity of sulfide. In this case, CO_2 content in MOF-74-Zn reaches 69% and the SO_2 content is about 31%. It also coincides with that of zMOF in the CH_4—CO_2—H_2S system.

Table 3 lists the recommended porous materials for removal of sulfide only, as well as removal of sulfide and CO_2 simultaneously. We can see that the optimum adsorbent is strongly dependent on the factors of the fluid systems and purification aims. Despite that zMOF is found to be the most suitable for removal of carbon and sulfide, the very high cost of indium metal may preclude its application for large-scale gas processing. It is expected this problem would be gradually solved in the future. In summary, by using computer simulations instead of expensive experiments, the complex screening process of potential materials can be easily and rapidly accomplished.

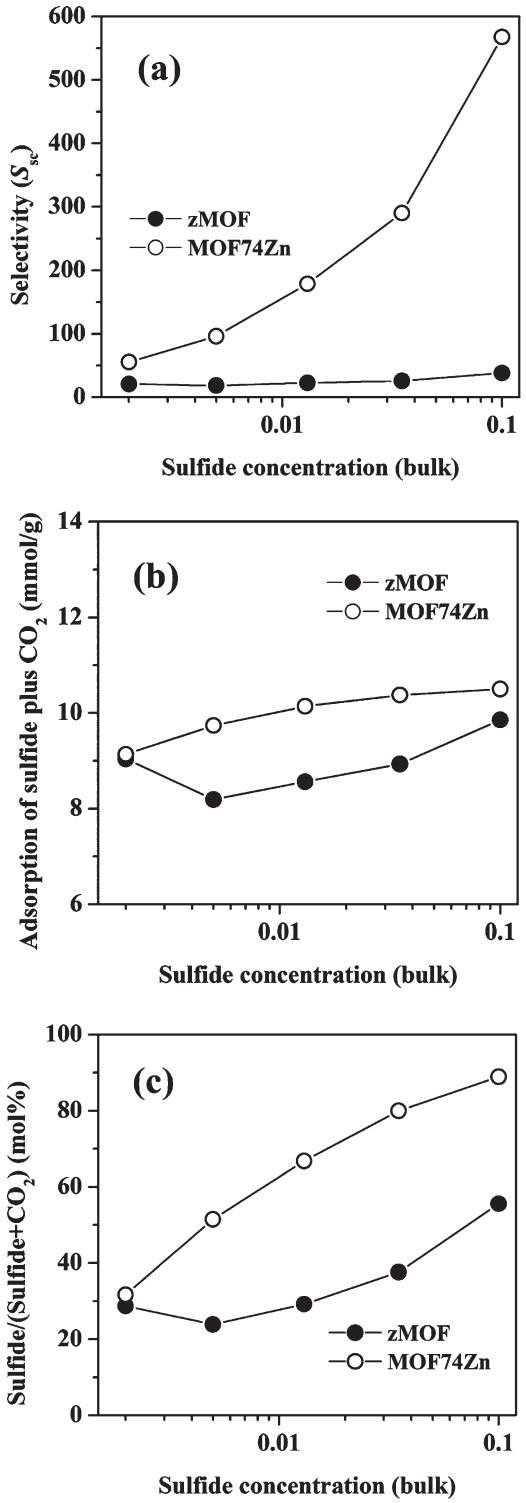

Figure 9. Effect of sulfide mole fraction in bulk phase on simultaneous removal of sulfide and CO_2 in the recommended porous materials at 4 MPa, where the closed and open symbols denote the CH_4—CO_2—H_2S and N_2—CO_2—SO_2 systems, respectively.

Effect of temperature on the selectivities and uptakes of screened adsorbents

Figure 6 shows the effect of temperature on the desulfurization of the CH_4—CO_2—H_2S and N_2—CO_2—SO_2 systems by the recommended adsorbents. For consistence with previous discussion, we used the simulated adsorption data at 4 M Pa for analysis. It is well known that increasing the temperature will usually reduce the selectivity. To our surprise, with the increase of temperature, a rising of selectivity occurs in both zeolites after a prior decrease (see Figure 6a). Figure 6b shows that the sulfide uptakes fall down slowly with the temperature. Hence, this rising can only be explained by the uptakes of other components like CO_2 decreasing sharper than sulfide. In contrast to zeolites, the adsorptions in MOFs are more noticeably influenced by the temperature. For instance, in the N_2—CO_2—SO_2 system, the selectivity and uptake of MIL-47(V) give a drop of 92% and 95%, respectively, whereas for Na-13X it declines only 35% and 52% in the whole temperature range. From the standpoint of adsorbent regeneration, zeolites are clearly inferior to MOFs, because desorbing sulfide at a higher temperature will spend a more energy consuming. Especially, only given a slight increase of temperature (from 303 K increasing to 333 K), the H_2S molecules are almost totally desorbed from the zMOF adsorbent. In this regard, zMOF is preeminent over other adsorbents and temperature swing adsorption is preferred for the removal of trace H_2S impurities in zMOF. Figure 7a and b show that increasing temperature leads to a quick decrease of the selectivity and uptake of SO_2 and CO_2 in MOF-74-Zn, in contrast to a moderate decline in zMOF for simultaneous removal of H_2S and CO_2. This phenomenon can also be interpreted by the corresponding variation trends of sulfide percentage in Figure 7c.

Effect of sulfide concentration on the selectivities and uptakes of recommended adsorbents

In general, the amount of sulfur (like H_2S) in raw natural gas varies widely from parts per million levels up to 5%. Hence, it is necessary to explore the effect of the sulfide concentration on the separation performance of recommended adsorbents. Figures 8 and 9 show the dependence of the selectivity and uptake on sulfide concentration of bulk phase for removal of sulfide and simultaneous removal of sulfide and CO_2, respectively. In both cases, the content of CH_4 or N_2 is fixed and we only increase the concentration of sulfide. We can see from Figure 8a when the bulk concentration of sulfide increases from 0.002 to 0.1, the selectivities of sulfide in both zeolites go down drastically and only give 1/70–1/80 of the original value. However, the uptakes of sulfide are nearly unchanged within the sulfide concentration range studied (see Figure 8b). According to Eq. 2, the change of sulfide bulk concentration will cut the selectivity to 1/50 of the original value. This implies that another contribution to this decrease arises from the increase of the total uptake of CH_4 and CO_2. As shown in Figure 8c, the selectivity of MOFs for sulfide also descends with the increase of sulfide concentration, but with a relatively slow rate, compared to zeolites. Fortunately, the sulfur storage capacity of MOFs would double at a high sulfide concentration, despite sacrificing selectivity. All these observations indicate that MOFs offer an obvious advantage over zeolites for the gas purification containing high levels of sulfide contaminant.

Figure 9a shows that for simultaneous desulfurization and decarburization, there is a significant difference between the selectivities of MOF-74-Zn and zMOF. Apparently, the selectivity of MOF-74-Zn suddenly ascends with the bulk sulfide content, whereas it is almost unaltered for zMOF. Because the gas composition of CH_4 or N_2 in each system is fixed, the

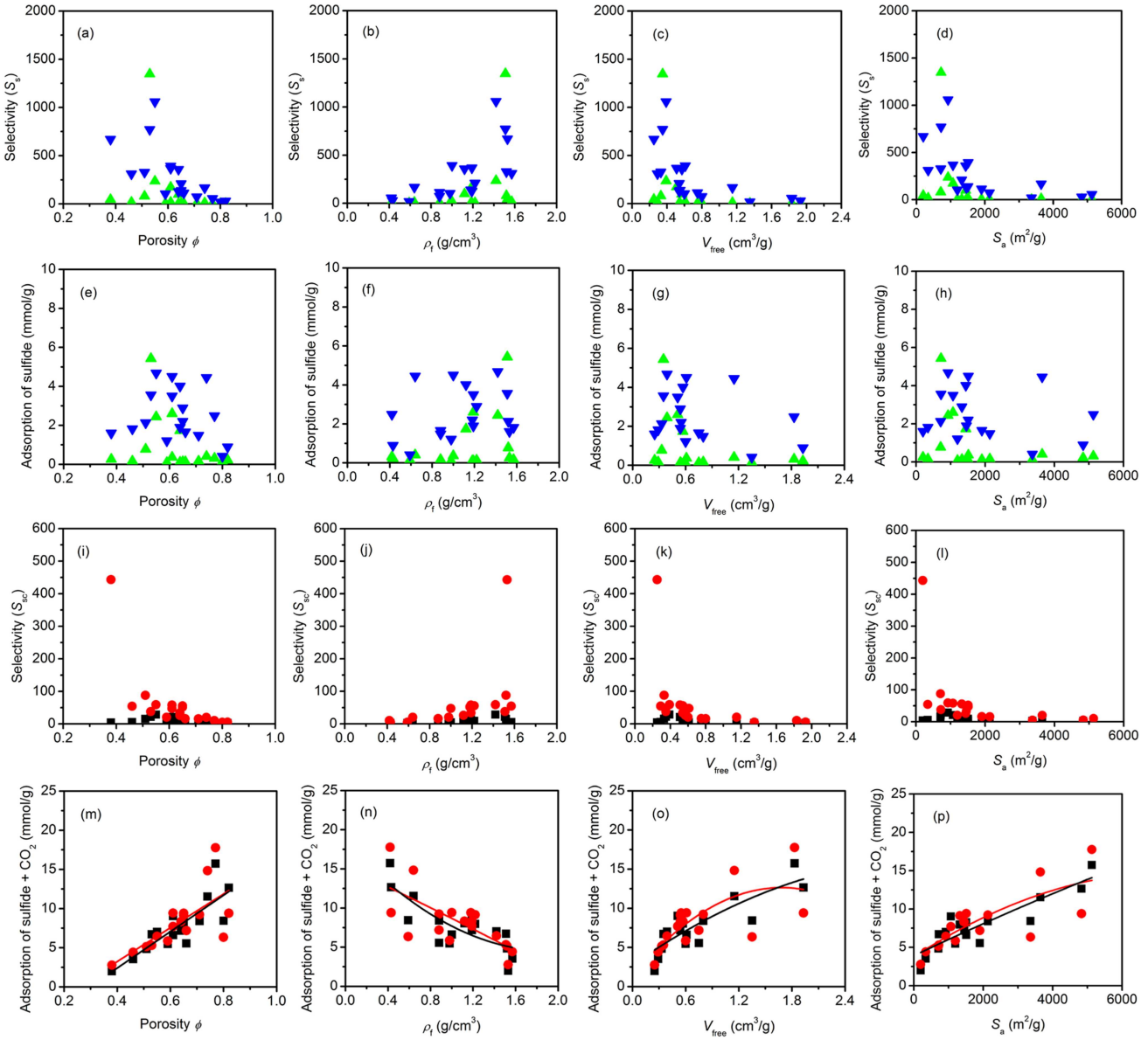

Figure 10. Adsorption selectivity and uptake versus porosity Φ, framework density ρ_f, free pore volume V_{free}, and accessible surface area S_a at 4 MPa and 303 K, where the pyramid symbol denotes removal of sulfide for CH_4—CO_2—H_2S, the inverted pyramid symbol denotes removal of sulfide for N_2—CO_2—SO_2, the square symbol denotes removal of sulfide and CO_2 for CH_4—CO_2—H_2S, and the circle symbol denotes removal of sulfide and CO_2 for N_2—CO_2—SO_2. Lines are the guide to the eyes.

[Color figure can be viewed in the online issue, which is available at wileyonlinelibrary.com.]

change of bulk sulfide content would not affect the molar ratio of the gas components in Eq. 3. With the increase of bulk sulfide concentration, the total uptake of sulfide and CO_2 in MOF-74-Zn increases monotonically (see Figure 9b). Furthermore, the percentage of sulfide in the total uptake increases pronouncedly. On the contrary, the total uptake of sulfide and CO_2 in zMOF exhibits a decrease trend and then increases with the increase of bulk sulfide concentration (see Figure 9b). The similar behavior also appears in the curve of the percentage of sulfide in the total uptake of zMOF (see Figure 9c).

Effect of material structure on the selectivities and uptakes of recommended adsorbents

To explore the effect of material structure on the separation ability of various adsorbents, the selectivities and uptakes at 4 MPa are plotted in Figure 10 as a function of the porosity Φ, framework density ρ_f, free pore volume V_{free}, and accessible surface area S_a. We can see that the optimum porosities Φ for desulfurization center on about 0.5–0.6, where both the selectivity and uptake are the highest. Furthermore, a large framework density ρ_f (~1.5 g cm^{-3}), and a small free pore volume V_{free} (~0.3 cm^3 g^{-1}) and accessible surface area S_a (~800 m^2 g^{-1}) benefit to the removal of trace sulfide. For desulfurization and decarburization simultaneously, the optimum porosities Φ is also found at 0.5–0.6 for their selectivities. However, the adsorption capacities of sulfide and CO_2 are favored at high porosities. The effects of framework density ρ_f, free pore volume V_{free}, and accessible surface area S_a on the selectivities of desulfurization/decarburization are similar to the case of desulfurization only.

Moreover, the uptakes of sulfide and CO_2 monotonically increase with the porosities Φ, free pore volume V_{free}, and accessible surface area S_a, but decrease with the increase of framework density ρ_f, which is consistent with the pure CO_2 storage in MOFs by Babarao and Jiang.[38] Clearly, the impact of material structure on separation performance is dependent on the different aims at the applications of desulfurization only and simultaneous desulfurization/decarburization.

Conclusions

We have performed a systematic molecular screening for porous carbons, zeolites, and MOFs to remove the sulfide and CO_2 from the ternary mixtures. It is found that for desulfurization only, zeolites are superior to carbons and MOFs, while for simultaneous desulfurization and decarburization, MOFs are better than zeolites and carbons. For both applications, the MOF adsorbents are easier to regeneration than zeolites, because the adsorbed gases can be released quickly by increasing temperature. In addition, the selectivities of MOFs decline slower with the increase of sulfide concentration in bulk phase, compared to zeolites. On the contrary, the uptakes of MOFs increase more evidently than zeolites. It demonstrates that the MOFs are more suitable for the desulfurization of gas containing high concentration contaminant. The effects of material structure on the selectivities and uptakes of the recommended adsorbents have also been discussed. In summary, this work proposed a computational strategy to screen the known materials for gas separation in ternary mixtures. More importantly, by using this strategy, unknown materials can also be rapidly screened without expensive experiments. It is expected that the information obtained would provide a deep insight into materials and process design, development, and operating optimization in subsequent applications.

Acknowledgments

This work was supported by the Open Project of State Key Laboratory of Clean Energy Utilization, Zhejiang University (No. ZJUCEU2010020), the Open Project of State Key Laboratory of Chemical Engineering (SKL-Che-12C01), National Basic Research Program of China (2011CB706900), NSF of China (No. 21121064), and the Chemical Grid Project of Beijing University of Chemical Technology.

Literature Cited

1. Belmabkhout Y, Sayari A. Isothermal versus non-isothermal adsorption−desorption cycling of triamine-grafted pore-expanded MCM-41 mesoporous silica for CO_2 capture from flue gas. *Energy Fuels*. 2010;24:5273–5280.
2. Peng X, Cao D, Zhao J. Grand canonical Monte Carlo simulation of methane–carbon dioxide mixtures on ordered mesoporous carbon CMK-1. *Sep Purif Technol*. 2009;68:50–60.
3. Peng X, Wang W, Xue R, Shen Z. Adsorption separation of CH_4/CO_2 on mesocarbon microbeads: experiment and modeling. *AIChE J*. 2006;52:994–1003.
4. Crespo D, Qi G, Wang Y, Yang FH, Yang RT. Superior sorbent for natural gas desulfurization. *Ind Eng Chem Res*. 2008;47:1238–1244.
5. Alonso-Vicario A, Ochoa-Gómez JR, Gil-Río S, Gómez-Jiménez-Aberasturi O, Ramírez-López CA, Torrecilla-Soria J, Domínguez A. Purification and upgrading of biogas by pressure swing adsorption on synthetic and natural zeolites. *Micropor Mesopor Mater*. 2010;134:100–107.
6. Cosoli P, Ferrone M, Pricl S, Fermeglia M. Hydrogen sulphide removal from biogas by zeolite adsorption: Part I. GCMC molecular simulations. *Chem Eng J*. 2008;145:86–92.
7. Bhandari DA, Bessho N, Koros WJ. Hollow fiber sorbents for desulfurization of natural gas. *Ind Eng Chem Res*. 2010;49:12038–12050.
8. Gollakota SV, Chriswell CD. Study of an adsorption process using silicalite for sulfur dioxide removal from combustion gases. *Ind Eng Chem Res*. 1988;27:139–143.
9. Yan R, Ng YL, Liang DT, Lim CS, Tay JH. Bench-scale experimental study on the effect of flue gas composition on mercury removal by activated carbon adsorption. *Energy Fuels*. 2003;17:1528–1535.
10. Sowers SL, Gubbins KE. Optimizing removal of trace components from nitrogen/X mixtures using adsorption: theory and simulation. *Langmuir*. 1995;11:4758–4764.
11. Ozturk B, Yildirim Y. Investigation of sorption capacity of pumice for SO_2 capture. *Process Saf Environ Prot*. 2008;86:31–36.
12. Iijima S. Helical microtubules of graphitic carbon. *Nature*. 1991;354:56–58.
13. Peng X, Cao D, Wang W. Heterogeneity characterization of ordered mesoporous carbon adsorbent CMK-1 for methane and hydrogen storage: GCMC simulation and comparison with experiment. *J Phys Chem C*. 2008;112:13024–13036.
14. Peng X, Cao D, Wang W. Computational characterization of hexagonally ordered carbon nanopipes CMK-5 and structural optimization for H_2 storage. *Langmuir*. 2009;25:10863–10872.
15. Peng X, Cao D, Wang W. Computational study on purification of CO_2 from natural gas by C_{60} intercalated graphite. *Ind Eng Chem Res*. 2010;49:8787–8796.
16. Peng X, Cao D, Wang W. Adsorption and separation of CH_4/CO_2/N_2/H_2/CO mixtures in hexagonally ordered carbon nanopipes CMK-5. *Chem Eng Sci*. 2011;66:2266–2276.
17. Peng X, Zhou J, Wang W, Cao D. Computer simulation for storage of methane and capture of carbon dioxide in carbon nanoscrolls by expansion of interlayer spacing. *Carbon*. 2010;48:3760–3768.
18. Akten ED, Siriwardane R, Sholl DS. Monte Carlo simulation of single- and binary-component adsorption of CO_2, N_2, and H_2 in zeolite Na-4A. *Energy Fuels*. 2003;17:977–983.
19. Demontis P, Gulín-González J, Jobic H, Suffritti GB. Diffusion of water in zeolites Na A and NaCa A: a molecular dynamics simulation study. *J Phys Chem C*. 2010;114:18612–18621.
20. Faux DA, Smith W, Forester TR. Molecular dynamics studies of hydrated and dehydrated Na+-Zeolite-4A. *J Phys Chem B*. 1997;101:1762–1768.
21. García-Sańchez A, Ania CO, Parra JB, Dubbeldam D, Vlugt TJH, Krishna R, Calero Sa. Transferable force field for carbon dioxide adsorption in zeolites. *J Phys Chem C*. 2009;113:8814–8820.
22. Goj A, Sholl DS, Akten ED, Kohen D. Atomistic simulations of CO_2 and N_2 adsorption in silica zeolites: the impact of pore size and shape. *J Phys Chem B*. 2002;106:8367–8375.
23. Granato MA, Lamia N, Vlugt TJH, Rodrigues ArE. Adsorption equilibrium of isobutane and 1-butene in zeolite 13X by molecular simulation. *Ind Eng Chem Res*. 2008;47:6166–6174.
24. Granato MA, Vlugt TJH, Rodrigues AE. Molecular simulation of propane−propylene binary adsorption equilibrium in zeolite 13X. *Ind Eng Chem Res*. 2007;46:7239–7245.
25. Punnathanam S, Denayer JFM, Daems I, Baron GV, Snurr RQ. Parallel tempering simulations of liquid-phase adsorption of n-alkane mixtures in zeolite LTA-5A. *J Phys Chem C*. 2011;115:762–769.
26. Subramanian V, Seff K. A near zero coordinate sodium ion in dehydrated zeolite 4A, Na12-A. *J Phys Chem*. 1977;81:2249–2251.
27. Wu JY, Liu QL, Xiong Y, Zhu AM, Chen Y. Molecular simulation of water/alcohol mixtures' adsorption and diffusion in zeolite 4A membranes. *J Phys Chem B*. 2009;113:4267–4274.
28. Chui SSY, Lo SMF, Charmant JPH, Orpen AG, Williams ID. A chemically functionalizable nanoporous material $[Cu_3(TMA)_2(H_2O)_3]$n. *Science*. 1999;283:1148–1150.
29. Eddaoudi M, Kim J, Rosi N, Vodak D, Wachter J, O'Keeffe M, Yaghi OM. Systematic design of pore size and functionality in isoreticular MOFs and their application in methane storage. *Science*. 2002;295:469–472.
30. D'Alessandro DM, Smit B, Long JR. Carbon dioxide capture: prospects for new materials. *Angew Chem Int Ed*. 2010;49:6058–6082.
31. Keskin S, Liu J, Rankin RB, Johnson JK, Sholl DS. Progress, opportunities, and challenges for applying atomically detailed modeling to molecular adsorption and transport in metal−organic framework materials. *Ind Eng Chem Res*. 2008;48:2355–2371.
32. Han SS, Mendoza-Cortes JL, Goddard Iii WA. Recent advances on simulation and theory of hydrogen storage in metal-organic

frameworks and covalent organic frameworks. *Chem Soc Rev*. 2009;38:1460–1476.
33. Czaja AU, Trukhan N, Muller U. Industrial applications of metal-organic frameworks. *Chem Soc Rev*. 2009;38:1284–1293.
34. Duren T, Bae Y-S, Snurr RQ. Using molecular simulation to characterise metal-organic frameworks for adsorption applications. *Chem Soc Rev*. 2009;38:1237–1247.
35. Xiang Z, Cao D, Lan J, Wang W, Broom DP. Multiscale simulation and modelling of adsorptive processes for energy gas storage and carbon dioxide capture in porous coordination frameworks. *Energy Environmental Science*.2010;3:1469–1487.
36. Li J-R, Kuppler RJ, Zhou H-C. Selective gas adsorption and separation in metal-organic frameworks. *Chem Soc Rev*. 2009;38:1477–1504.
37. Xiang ZH, Hu Z, Cao DP, Yang WT, Lu J, Han B, Wang WC. Metal-organic frameworks with incorporated carbon nanotubes: improving CO_2 and CH_4 storage capacities by lithium doping. *Angew Chem Int Ed*. 2011;50:491–494.
38. Babarao R, Jiang J. Molecular screening of metal−organic frameworks for CO_2 storage. *Langmuir*. 2008;24:6270–6278.
39. Yazaydın AOzr, Snurr RQ, Park T-H, Koh K, Liu J, LeVan MD, Benin AI, Jakubczak P, Lanuza M, Galloway DB, Low JJ, Willis RR. Screening of metal–organic frameworks for carbon dioxide capture from flue gas using a combined experimental and modeling approach. *J American Chem Soc*. 2009;131:18198–18199.
40. Hamon L, Leclerc H, Ghoufi A, Oliviero L, Travert A, Lavalley J-C, Devic T, Serre C, Férey Gr, De Weireld G, Vimont A, Maurin G. Molecular insight into the adsorption of H_2S in the flexible MIL-53(Cr) and rigid MIL-47(V) MOFs: infrared spectroscopy combined to molecular simulations. *J Phys Chem C*. 2011;115:2047–2056.
41. Hamon L, Serre C, Devic T, Loiseau T, Millange F, Férey Gr, Weireld GD. Comparative study of hydrogen sulfide adsorption in the MIL-53(Al, Cr, Fe), MIL-47(V), MIL-100(Cr), and MIL-101(Cr) metal−organic frameworks at room temperature. *J Am Chem Soc*. 2009;131:8775–8777.
42. Liu B, Smit B. Comparative molecular simulation study of CO_2/N_2 and CH_4/N_2 separation in zeolites and metal−organic frameworks. *Langmuir*. 2009;25:5918–5926.
43. Herm ZR, Swisher JA, Smit B, Krishna R, Long JR. Metal−organic frameworks as adsorbents for hydrogen purification and precombustion carbon dioxide capture. *J Am Chem Soc*. 2011;133:5664–5667.
44. Myers AL, Prausnitz JM. Thermodynamics of mixed-gas adsorption. *AIChE J*. 1965;11:121–127.
45. Belmabkhout Y, Heymans N, De Weireld G, Sayari A. Simultaneous adsorption of H_2S and CO_2 on triamine-grafted pore-expanded mesoporous MCM-41 silica. *Energy Fuels*. 2011;25:1310–1315.
46. Wang W, Peng X, Cao D. Capture of trace sulfur gases from binary mixtures by single-walled carbon nanotube arrays: a molecular simulation study. *Environ Sci Technol*. 2011;45:4832–4838.
47. Calero S, Dubbeldam D, Krishna R, Smit B, Vlugt TJH, Denayer JFM, Martens JA, Maesen TLM. Understanding the role of sodium during adsorption: a force field for alkanes in sodium-exchanged faujasites. *J Am Chem Soc*. 2004;126:11377–11386.
48. Pluth JJ, Smith JV. Accurate redetermination of crystal structure of dehydrated zeolite A. Absence of near zero coordination of sodium. Refinement of silicon,aluminum-ordered superstructure. *J Am Chem Soc*. 1980;102:4704–4708.
49. García-Pérez E, Dubbeldam D, Maesen TLM, Calero S. Influence of cation Na/Ca ratio on adsorption in LTA 5A: a systematic molecular simulation study of alkane chain length. *J Phys Chem B*. 2006;110:23968–23976.
50. Yaghi OM, O'Keeffe M, Ockwig NW, Chae HK, Eddaoudi M, Kim J. Reticular synthesis and the design of new materials. *Nature*. 2003;423:705–714.
51. Barthelet K, Marrot J, Riou D, Férey G. A breathing hybrid organic–inorganic solid with very large pores and high magnetic characteristics. *Angew Chem Int Ed*. 2002;41:281–284.
52. Rosenbach N, Jobic H, Ghoufi A, Salles F, Maurin G, Bourrelly S, Llewellyn PL, Devic T, Serre C, Férey G. Quasi-elastic neutron scattering and molecular dynamics study of methane diffusion in metal organic frameworks MIL-47(V) and MIL-53(Cr). *Angew Chem Int Ed*. 2008;47:6611–6615.
53. Chae HK, Siberio-Perez DY, Kim J, Go Y, Eddaoudi M, Matzger AJ, O'Keeffe M, Yaghi OM. A route to high surface area, porosity and inclusion of large molecules in crystals. *Nature*. 2004;427:523–527.
54. Millward AR, Yaghi OM. Metal−organic frameworks with exceptionally high capacity for storage of carbon dioxide at room temperature. *J Am Chem Soc*. 2005;127:17998–17999.
55. Côté AP, Benin AI, Ockwig NW, O'Keeffe M, Matzger AJ, Yaghi OM. Porous, crystalline, covalent organic frameworks. *Science*. 2005;310:1166–1170.
56. El-Kaderi HM, Hunt JR, Mendoza-Cortés JL, Côté AP, Taylor RE, O'Keeffe M, Yaghi OM. Designed synthesis of 3D covalent organic frameworks. *Science*. 2007;316:268–272.
57. Cao DP, Lan J, Wang WC, Smit B. Li-doped 3D covalent organic frameworks: high capacity hydrogen storage materials. *Angew Chem Int Ed*. 2009;48:4730.
58. Lan JH, Cao DP, Wang WC, Smit B. Doping of alkali, alkaline-earth and transition metals in covalent-organic frameworks for enhancing CO_2 capture by first-principles calculations and molecular simulations. *ACS Nano*. 2010;4:4225–4237.
59. Lin X, Telepeni I, Blake AJ, Dailly A, Brown CM, Simmons JM, Zoppi M, Walker GS, Thomas KM, Mays TJ, Hubberstey P, Champness NR, Schröder M. High capacity hydrogen adsorption in Cu(II) tetracarboxylate framework materials: the role of pore size, ligand functionalization, and exposed metal sites. *J Am Chem Soc*. 2009;131:2159–2171.
60. Park KS, Ni Z, Côté AP, Choi JY, Huang R, Uribe-Romo FJ, Chae HK, O'Keeffe M, Yaghi OM. Exceptional chemical and thermal stability of zeolitic imidazolate frameworks. *Proc Natl Acad Sci*. 2006;103:10186–10191.
61. Banerjee R, Phan A, Wang B, Knobler C, Furukawa H, O'Keeffe M, Yaghi OM. High-throughput synthesis of zeolitic imidazolate frameworks and application to CO_2 capture. *Science*. 2008;319:939–943.
62. Keskin S. Atomistic simulations for adsorption, diffusion, and separation of gas mixtures in zeolite imidazolate frameworks. *J Phys Chem C*. 2010;115:800–807.
63. Morris W, Leung B, Furukawa H, Yaghi OK, He N, Hayashi H, Houndonougbo Y, Asta M, Laird BB, Yaghi OM. A combined experimental−computational investigation of carbon dioxide capture in a series of isoreticular zeolitic imidazolate frameworks. *J Am Chem Soc*. 2010;132:11006–11008.
64. Rosi NL, Kim J, Eddaoudi M, Chen B, O'Keeffe M, Yaghi OM. Rod packings and metal−organic frameworks constructed from rod-shaped secondary building units. *J Am Chem Soc*. 2005;127:1504–1518.
65. Britt D, Tranchemontagne D, Yaghi OM. Metal-organic frameworks with high capacity and selectivity for harmful gases. *Proc Natl Acad Sci*. 2008;105:11623–11627.
66. Zhou W, Wu H, Yildirim T. Enhanced H_2 adsorption in isostructural metal−organic frameworks with open metal sites: strong dependence of the binding strength on metal ions. *J Am Chem Soc*. 2008;130:15268–15269.
67. Grant Glover T, Peterson GW, Schindler BJ, Britt D, Yaghi O. MOF-74 building unit has a direct impact on toxic gas adsorption. *Chem Eng Sci*. 2011;66:163–170.
68. Liu Y, Eubank JF, Cairns AJ, Eckert J, Kravtsov VC, Luebke R, Eddaoudi M. Assembly of metal–organic frameworks (MOFs) based on indium-trimer building blocks: a porous MOF with soc topology and high hydrogen storage. *Angew Chem Int Ed*. 2007;46:3278–3283.
69. Liu Y, Kravtsov VC, Larsen R, Eddaoudi M. Molecular building blocks approach to the assembly of zeolite-like metal-organic frameworks (ZMOFs) with extra-large cavities. *Chem Commun*. 2006:1488–1490.
70. Babarao R, Jiang J, Sandler SI. Molecular simulations for adsorptive separation of CO_2/CH_4 mixture in metal-exposed, catenated, and charged metal−organic frameworks. *Langmuir*. 2008;25:5239–5247.
71. Babarao R, Jiang J. Unprecedentedly high selective adsorption of gas mixtures in rho zeolite-like metal−organic framework: a molecular simulation study. *J Am Chem Soc*. 2009;131:11417–11425.
72. Hunger J, Beta IA, Böhlig H, Ling C, Jobic H, Hunger B. Adsorption structures of water in NaX studied by DRIFT spectroscopy and neutron powder diffraction. *J Phys Chem B*. 2006;110:342–353.
73. Babarao R, Jiang J. Exceptionally high CO_2 storage in covalent-organic frameworks: atomistic simulation study. *Energy Environ Sci*. 2008;1:139–143.
74. Thomson KT, Gubbins KE. Modeling structural morphology of microporous carbons by reverse Monte Carlo. *Langmuir*. 2000;16:5761–5773.

75. Düren T, Millange F, Férey G, Walton KS, Snurr RQ. Calculating geometric surface areas as a characterization tool for metal−organic frameworks. *J Phys Chem C*. 2007;111:15350–15356.
76. Peng X, Cheng X, Cao D. Computer simulations for the adsorption and separation of $CO_2/CH_4/H_2/N_2$ gases by UMCM-1 and UMCM-2 metal organic frameworks. *J Mater Chem*. 2011;21:11259–11270.
77. Babarao R, Hu Z, Jiang J, Chempath S, Sandler SI. Storage and separation of CO_2 and CH_4 in silicalite, C_{168} schwarzite, and IRMOF-1: a comparative study from Monte Carlo simulation. *Langmuir*. 2006;23:659–666.
78. Ohkubo T, Miyawaki J, Kaneko K, Ryoo R, Seaton NA. Adsorption properties of templated mesoporous carbon (CMK-1) for nitrogen and supercritical methane experiment and GCMC simulation. *J Phys Chem B*. 2002;106:6523–6528.
79. Harris JG, Yung KH. Carbon dioxide's liquid-vapor coexistence curve and critical properties as predicted by a simple molecular model. *J Phys Chem*. 1995;99:12021–12024.
80. Peng X, Zhao J, Cao D. Adsorption of carbon dioxide of 1-site and 3-site models in pillared clays: a Gibbs ensemble Monte Carlo simulation. *J Colloid Interface Sci*. 2007;310:391–401.
81. Nath SK. Molecular simulation of vapor−liquid phase equilibria of hydrogen sulfide and its mixtures with alkanes. *J Phys Chem B*. 2003;107:9498–9504.
82. Ribeiro MCC. Molecular dynamics simulation of liquid sulfur dioxide. *J Phys Chem B*. 2006;110:8789–8797.
83. Ohba T, Kojima N, Kanoh H, Kaneko K. Unique hydrogen-bonded structure of water around Ca ions confined in carbon slit pores. *J Phys Chem C*. 2009;113:12622–12624.
84. Rappe AK, Casewit CJ, Colwell KS, Goddard WA, Skiff WM. UFF, a full periodic table force field for molecular mechanics and molecular dynamics simulations. *J Am Chem Soc*. 1992;114:10024–10035.
85. Gaussian 03, Revision C.02, Frisch MJ, Trucks GW, Schlegel HB, Scuseria GE, Robb MA, Cheeseman JR, Montgomery Jr, JA, Vreven T, Kudin KN, Burant JC, Millam JM, Iyengar SS, Tomasi J, Barone V, Mennucci B, Cossi M, Scalmani G, Rega N, Petersson GA, Nakatsuji H, Hada M, Ehara M, Toyota K, Fukuda R, Hasegawa J, Ishida M, Nakajima T, Honda Y, Kitao O, Nakai H, Klene M, Li X, Knox JE, Hratchian HP, Cross JB, Bakken V, Adamo C, Jaramillo J, Gomperts R, Stratmann RE, Yazyev O, Austin AJ, Cammi R, Pomelli C, Ochterski JW, Ayala PY, Morokuma K, Voth GA, Salvador P, Dannenberg JJ, Zakrzewski VG, Dapprich S, Daniels AD, Strain MC, Farkas O, Malick DK, Rabuck AD, Raghavachari K, Foresman JB, Ortiz JV, Cui Q, Baboul AG, Clifford S, Cioslowski J, Stefanov BB, Liu G, Liashenko A, Piskorz P, Komaromi I, Martin RL, Fox DJ, Keith T, Al-Laham MA, Peng CY, Nanayakkara A, Challacombe M, Gill PMW, Johnson B, Chen W, Wong MW, Gonzalez C, and Pople, JA, Gaussian, Inc., Wallingford CT, 2004.
86. Frenkel D, Smit B. Understanding Molecular Simulation: From Algorithms to Applications. New York: Academic Press, 2002.
87. Allen MP, Tildesley DJ. Computer Simulation of Liquids. Oxford University Press, USA, 1989.
88. Wolf D, Keblinski P, Phillpot SR, Eggebrecht J. Exact method for the simulation of Coulombic systems by spherically truncated, pairwise r[sup-1] summation. *J Chem Phys*. 1999;110:8254–8282.
89. Gupta A, Chempath S, Sanborn MJ, Clark LA, Snurr RQ. Object-oriented programming paradigms for molecular modeling. *Mol Simul*. 2003;29:29–46.
90. Peng D-Y, Robinson DB. A new two-constant equation of state. *Ind Eng Chem Fundam*. 1976;15:59–64.

Manuscript received Apr. 8, 2012, and revision received Oct. 2, 2012.